

Dalton Transactions

An international journal of inorganic chemistry

Accepted Manuscript

This article can be cited before page numbers have been issued, to do this please use: O. Abuzalat, S. Homayoonnia, D. Wong, H. R. Tantawy and S. Kim, *Dalton Trans.*, 2021, DOI: 10.1039/DODT04382F.



This is an Accepted Manuscript, which has been through the Royal Society of Chemistry peer review process and has been accepted for publication.

Accepted Manuscripts are published online shortly after acceptance, before technical editing, formatting and proof reading. Using this free service, authors can make their results available to the community, in citable form, before we publish the edited article. We will replace this Accepted Manuscript with the edited and formatted Advance Article as soon as it is available.

You can find more information about Accepted Manuscripts in the [Information for Authors](#).

Please note that technical editing may introduce minor changes to the text and/or graphics, which may alter content. The journal's standard [Terms & Conditions](#) and the [Ethical guidelines](#) still apply. In no event shall the Royal Society of Chemistry be held responsible for any errors or omissions in this Accepted Manuscript or any consequences arising from the use of any information it contains.

ARTICLE

Received 00th January 20xx,
Accepted 00th January 20xx

DOI: 10.1039/x0xx00000x

Facile and rapid synthesis of functionalized Zr-BTC for optical detection of blistering agent simulant 2-chloroethyl ethyl sulfide (CEES)

Osama Abuzalat ^{a,*}, Setareh Homayoonnia^b, Danny Wong^b, Hesham R Tantawy^a, Seonghwan Kim^{b,*}

2-chloroethyl ethyl sulfide (CEES) is a simulant for the chemical warfare agent, bis(2-chloroethyl) sulfide, also known as mustard gas. Here, we demonstrate a facile and rapid method to synthesize a functionalized metal-organic framework (MOF) material for the detection of CEES in trace level. While Zr-BTC is synthesized, in-situ encapsulation of fluorescent material (Fluorescein) into Zr-BTC voids is performed with a simple solvothermal reaction. The produced F@Zr-BTC is used as a fluorescent probe for CEES detections. The synthesized material shows fluorescence quenching under illumination at excitation wavelength of 470 nm when the F@Zr-BTC is exposed to CEES. This sensing material shows the highest fluorescence quenching at an emission wavelength of 534 nm with CEES concentration as low as 50 ppb. Therefore, the demonstrated sensing method with F@Zr-BTC offers a fast and convenient protocol for selective and sensitive detection of CEES in practical applications.

1. Introduction

Chemical warfare agents (CWAs) are toxic chemical substances used to kill and injure human beings in battlefields. Sulfur Mustard [bis(2-chloroethyl) sulfide] (SM), also known as mustard gas or HD, is one of the most infamous type of CWAs. Since World War I, it has been highly used in battlefields and caused about 70% of the casualties who suffered from toxic gases during the war.¹ SM causes severe ocular injury, respiratory disorders, severe debilitating injuries to the lungs and other organs, as well as erythema and blisters on the skin.² Besides, it may even have an effect on the division of cells by irreversibly alkylating the DNA, RNA, and proteins,³ and in some cases may lead to death.⁴

For the laboratory studies, simulants which structurally are similar to CWAs but less virulent are commonly used due to the high level of toxicity of the life-threatening CWAs.⁵ 2-chloroethyl ethyl sulfide (CEES), called half mustard, is the commercial simulant of SM which has less terminal chlorine content than SM. Therefore, it is less toxic than SM, but its DNA alkalization and vesicant properties are still similar to mustard gas.²

The risk of human exposure to SM in terrorist attacks is rising due to its low cost of preparation, elementary technology and equipment used to synthesize, no need for advanced knowledge on this specific subject, and stockpiling feasibility.⁶ Unfortunately, there are no effective antitoxins or treatments for injury which results from SM,⁴ and despite an international ban, very recently, SM was used in the conflict in Syria.⁷ Thus,

there is an urgent need for the development of facile techniques to detect CWAs rapidly in the field. To date, techniques such as gas chromatography-mass spectrometry,⁸ ion mobility spectrometry,⁹ Raman spectroscopy,¹⁰ calorimetric infrared (IR) spectroscopy,¹¹ and proton-transfer-reaction mass spectrometry¹² have been used to detect CWAs. However, they are not appropriate for field applications in warfare due to bulky instrumentation and time-consuming, complex operations. On the other end of the spectrum, chemically doped-CWAs detection papers such as M8, M9 and DB-3, which are used by the US military, are cheap, portable and easy to use, but are relatively insensitive, non-specific, and prone to false positives.¹³

For on-site detection of CWAs, there are many handheld chemical agent detectors which recognize CWAs based on their weight, volatility, and presence of sulfur or phosphorus, but generally they are partially selective in detection which cause false positive alarms.¹⁴ Recently, nanomaterials-based sensors have also been used for detection of CEES, such as Al-doped ZnO quantum dot sensor coupled with a packed column for gas chromatography¹ and ZnO nanoparticles-based resistive sensor¹⁵, due to the advantages of small grain size and large surface area of nanomaterials.

The chemistry of CWAs and their simulants on various heterogeneous surfaces, such as zeolites, transition metal oxides and activated carbons, has been investigated in extensive studies.^{16, 17} Although these porous materials showed desirable characteristics for detection and destruction of CWAs, they do not have tailorability, selectivity, reversibility, and high sorption capacity. Therefore, there is an urgent need for finding better suitable materials that provide required functionalities for detection and destruction of CWAs.¹⁸

New class of crystalline porous materials, called metal-organic frameworks (MOFs), developed in the last two decades are promising candidates for the detoxification or detection of CWAs due to their interesting structures and properties.¹⁹⁻²¹ Hypothetically, MOFs show superior advantages in this regard

^a Department of Chemical Engineering, Military Technical College, Cairo, Egypt

^b Department of Mechanical and Manufacturing Engineering, University of Calgary, Calgary, Alberta T2N 1N4, Canada

ARTICLE

Journal Name

due to: 1) ultra-high active surface area, 2) relatively infinite volume and unlimited reactive sites for functional group catalysis due to their isoreticular 3D structure, 3) possibility to engineer pore size on the scale of nano, meso, and microscale to adsorb complex CAs molecules, 4) capability to tune and engineer the task specific metal ion centers to CAs molecules hydrolysis/catalysis chemistry, 5) chemical and thermal stability.^{18,22} To date, various types of MOFs have been used for detoxification of CAs,²³⁻²⁶ but there are only few studies on MOF-based sensing devices for detection of this family of compounds.²⁷ Although MOF-based sensors for CEES detection have not yet been developed, previous works demonstrated the suitability of MOFs as luminescent detectors for nitroaromatic explosives,²⁸⁻³⁰ dinitrotoluene,²⁹ and alkyl phosphonate compounds.²⁷

Among the various potential applications of MOFs, using them as the fluorescence sensing platform is of great promise because of their advantages, such as operability, reusability, rapid response, high sensitivity, and high selectivity.²⁷ The fluorescence sensing capability of MOFs is on basis of the interaction between their structures and the target molecules. In the sensing process, first, the target molecules are adsorbed on the MOF, and then the energy transfer between the target molecules and the MOF structure leads to the quenching of the emission.²⁸ The photoluminescence of MOFs can be emitted from the metal ions, ligand molecules or some guest molecules in the MOFs pores.³¹ In MOFs which are made with aromatic ligands, the π -electron systems of the ligands result in the MOFs' photoluminescence properties upon excitation.²⁸ Zr-BTC or MOF-808 is a Zirconium-based MOF that has aromatic BTC ligands (1,3,5-benzenetricarboxylate).³² To the best of our knowledge, here we demonstrate Zr-BTC encapsulated with fluorescent material (Fluorescein) as an optical sensor for CEES for the first time. The guest fluorescent material greatly enhances the fluorescence quenching properties of F@Zr-BTC towards CEES analytes. F@Zr-BTC exhibits high sensitivity and selectivity for CEES detection in trace level.

2. Materials and Methods

2.1 Materials

All chemicals are of analytical grade and used without further purification. Zirconium tetrachloride ($ZrCl_4$, 98%, VWR), Trimesic acid (1, 3, 5-benzenetricarboxylic acid, H3BTC, 98%, Alfa Aesar), N,N-Dimethylformamide (DMF, 99.8%, VWR), Fluorescein (F, 90%, VWR), Glacial acetic acid (98%, VWR), 2-chloroethyl ethyl sulfide (CEES, 97%, Sigma Aldrich), 2-mercapto ethanol (98%, VWR), Hydrogen sulfide saturated solution in water (H_2S , VWR), Dimethyl methyl phosphonate (DMMP, 98%, VWR), ethanol (98 %, VWR) and deionized water (DIW) are used as received.

2.2 Preparation of Precursor Solutions and Synthesis of Zr-BTC and F@Zr-BTC

Briefly, dissolving 0.2 g (0.50 mM) of $ZrCl_4$ and 0.07 g (0.15 mM) of 1,3,5-benzenetricarboxylic acid in 5 mL of acetic acid and 10 mL of N, N-Dimethylformamide in a closed vial. The mixture is stirred without heating for 15 minutes before being sealed and heated at 120 °C for 24 hours. The mixture is cooled to the room

temperature in the oven and then the resulting materials are recovered by centrifuge at 6000 rpm. Finally, the resulting precipitates are dried under vacuum at 80 °C for 4 hours. The same procedure is used to prepare F@Zr-BTC except adding 0.001 g of Fluorescein to the precursor solutions. The final product of F@Zr-BTC is separated by centrifuge at 6000 rpm then dried at 80 °C under vacuum overnight. To ensure that the guest species (F) are not left adhered to the MOF surface, the product is washed thoroughly twice using solvents that solubilize the guest species (first using DMF, followed by acetic acid, methanol, ethanol, and acetone). The washing step is carried out with simultaneous sonication (10 minutes per solvent, then centrifugation) to further expedite the removal of external guest species.

2.3 Materials Characterization Techniques

A field emission scanning electron microscope (FE-SEM, Quanta™ 250) is used to determine and analyze the morphologies of the Zr-BTC and F@Zr-BTC. An X-ray diffractometer (XRD, Rigaku Multiflex) is used to characterize the crystalline structure of the Zr-BTC and F@Zr-BTC. Fourier Transform Infrared Spectroscopy (FTIR) (Nicolet Nexus 470, USA) is used to measure the transmittance IR spectra in the range of 4000–500 cm^{-1} with a spectral resolution of 4 cm^{-1} . Raman spectroscopy (Bruker Raman II, Laser (1064 nm) Power 300 mW, USA) is used to measure the Raman spectra of Fluorescein, Zr-BTC, and F@Zr-BTC. The Brunauer-Emmett-Teller (BET) measurements are performed using a surface area analyzer (NOVA 3000e, USA) to determine the surface areas of Zr-BTC and F@Zr-BTC. Fluorescence spectra of Fluorescein, Zr-BTC, and F@Zr-BTC are measured with a UV-Vis spectrometer (Ocean Optics, Flame-S, USA).

2.4 Fluorescence measurements for selective sensing of CEES

To carry out the fluorescence titration for CEES, 10 mg of the finely ground F@Zr-BTC is added to 120 mL of ethanol. After the sonication of this mixture at room temperature for 30 min, a suspension of F@Zr-BTC in ethanol is obtained. Then 4.5 mL of the suspension is pipetted to a 5 mL volumetric flask; after that different amounts of CEES dilutes are added. The volume of the suspension containing CEES is adjusted to 5 mL by ethanol, giving a different concentration of CEES in the F@Zr-BTC fluorescent crystal probe suspension. Finally, this suspension is transferred to a quartz cuvette followed by monitoring emission intensity upon excitation at 470 nm using a UV-Vis spectrometer with a fluorescence measurement set up. It is worth mentioning here that Zr-BTC alone shows negligible responses to CEES.

3. Results and Discussion

In Zr-BTC (i.e. MOF-808), each Zr secondary building unit, $Zr_6O_4(OH)_4(-CO_2)_6(HCOO)_6$, is linked to six BTC units to form a 3D porous networks having two different types of pores. The smaller one is tetrahedral pore which is inaccessible to guests because of its small aperture diameter of 1.2 Å, while the larger one has a much larger internal void and aperture diameters of

18 and 14 Å, respectively.³³ The dimensions of Fluorescein molecules are estimated to be oblate with semi-axes of 7 Å and 2 Å for bond length and van der Waals radii³⁵ which are smaller than the larger pore and aperture diameter of Zr-BTC. As a result, Fluorescein molecules are geometrically favorable for encapsulation within the void space of Zr-BTC. The key point here is to choose suitable guest molecules that can be easily encapsulated in Zr-BTC voids. Fluorescein is one of the relatively smaller and yet highly fluorescent material.³⁵ Fluorescent Zr-BTC (F@Zr-BTC) nanocrystals could be formed by solvothermal synthesis (via simple mixing of BTC, F, and Zirconium tetrachloride solutions in DMF) in arrangement with the concept of in situ guest encapsulation as shown in Figure 1.

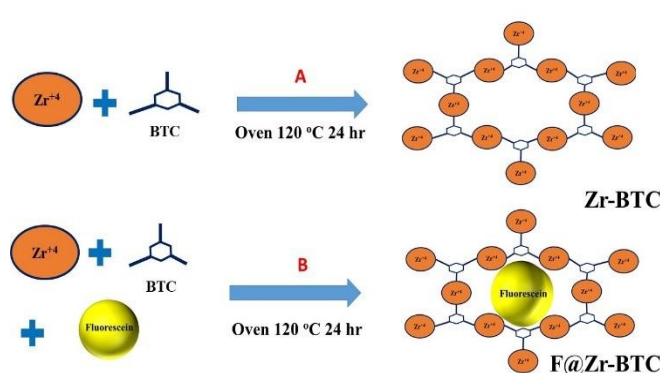


Figure 1. Schematic diagram illustrating the strategy of the in-situ encapsulation of Fluorescein guest in the Zr-BTC voids.

3.1 Morphological and structural characterization of Zr-BTC and F@Zr-BTC

Visual inspections indicate that white pure crystalline dried product, Zr-BTC, is obtained from the reaction of Zirconium tetrachloride with 1, 3, 5-benzenetricarboxylic acid. However, the reaction of Zirconium tetrachloride and Fluorescein with 1, 3, 5-benzenetricarboxylic acid yields yellow colour crystals of F@Zr-BTC. Scanning electron microscopy (SEM) confirms cubic morphology of Zr-BTC³⁶ and its average particle size in the range of 100 nm as shown in Figure 2(a). In contrast, we recognize that the encapsulation process of the Fluorescein guest within Zr-BTC has resulted in a relatively larger particle size distribution between 100 and 200 nm from Figure 2(b). We attribute that the supportive self-assembly of Fluorescein within Zr-BTC may have an effect on the growth rate of Zr-BTC nanocrystals. Therefore, the achieved crystallization of Zr-BTC under the conditions of Fluorescein encapsulation may be dominated by an initial fast nucleation followed by slow continuous growth. The obtained near constant cubic morphology is maintained throughout the growth process, which allows the potential to trap the guest Fluorescein successfully within the void space. Fluorescein may act as a modulator which promotes crystal growth which leads to the formation of larger crystals of F@Zr-BTC compared to Zr-BTC.³⁷⁻³⁹

Figure 3 presents the structural data of the Fluorescein (blue), pure Zr-BTC (black), and F@Zr-BTC (red). Powder X-ray diffraction (PXRD) patterns and simulated pattern in Figure 3(a)

show the structural crystallographic planes of Zr-BTC which match well with literature.^{36,40,41,42} The two sharp peaks at the 8.36° (311) and 8.74° (222) for the Zr-BTC reveal that the material obtained has high crystallinity. No separate ZrO₂ peaks are detected, which indicates good reproducibility of the MOF material⁴². We find that Zr-BTC has retained its pristine structural form, upon encapsulation with Fluorescein guest, for which no major structural changes have been observed between two PXRD patterns. However, we notice that slight intensity enhancement in case of F@Zr-BTC which may be attributed to a relatively larger crystal size distribution (degree of crystallinity). These results confirm the positive impact of Fluorescein encapsulation over crystallization as expected. Accordingly, these observed data confirm the successful Fluorescein encapsulation process.

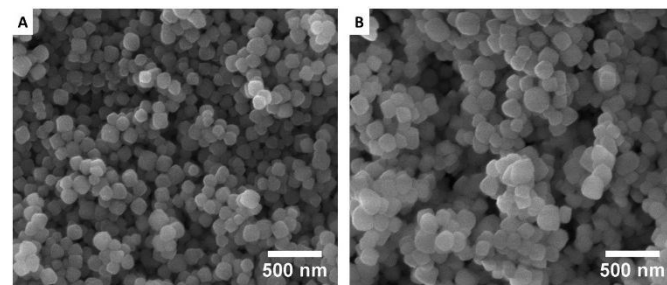


Figure 2. SEM images of (a) Zr-BTC and (b) F@Zr-BTC.

Vibrational spectroscopy data acquired by Raman spectroscopy are used in order to confirm the Zr-BTC structure. Figure 3(b) shows the Raman spectra of Fluorescein (blue), Zr-BTC (black), and F@Zr-BTC (red). The major Raman peaks of Zr-BTC are observed at 806 cm⁻¹ (Zr-O), 1012 cm⁻¹ (benzene ring deformation), 1370 cm⁻¹ (C-O stretching), 1456-1436 cm⁻¹ (OCO symmetric stretching in-phase), 1624 cm⁻¹ (C=C stretching of aromatic rings), 3078 cm⁻¹ (CH stretching).^{36, 43} Interestingly, Raman peaks of Fluorescein observed at 1139, 1186, 1418, 1510, and 1593 cm⁻¹ are completely absent from the spectrum of F@Zr-BTC. These results confirm that Fluorescein does not exist on the surface of Zr-BTC and hence support the successful encapsulation of Fluorescein. Functional group analysis by FTIR is also shown in Figure 3(c). C=O stretching vibrations were observed at 1720-1620 cm⁻¹. Peak at 1365 cm⁻¹ is assigned as stretching vibration of C-O group, indicating the deprotonation of carboxylate group of BTC and coordination with Zirconium (IV) metal ion to form Zr-BTC.⁴⁴ Peak at 3004 cm⁻¹ is related to C-H aromatic vibration bands in the synthesized Zr-BTC. The peak at 1578 cm⁻¹ is assigned with C=C bond in the aromatic ring. The vibration peak of Zr-O is observed at around 650 cm⁻¹, indicating that coordination reaction occurs between the carboxyl groups of BTC and zirconium ions.^{44, 45} Together we conclude that the Zr-BTC has retained its pure structural form, even upon encapsulation with Fluorescein guest, for which no major structural changes have been observed. This behavior is similar to examples shown in the literature which reported no change in the structural X-ray diffraction pattern upon guest molecule encapsulation in the MOF host compounds.⁴⁶⁻⁵¹

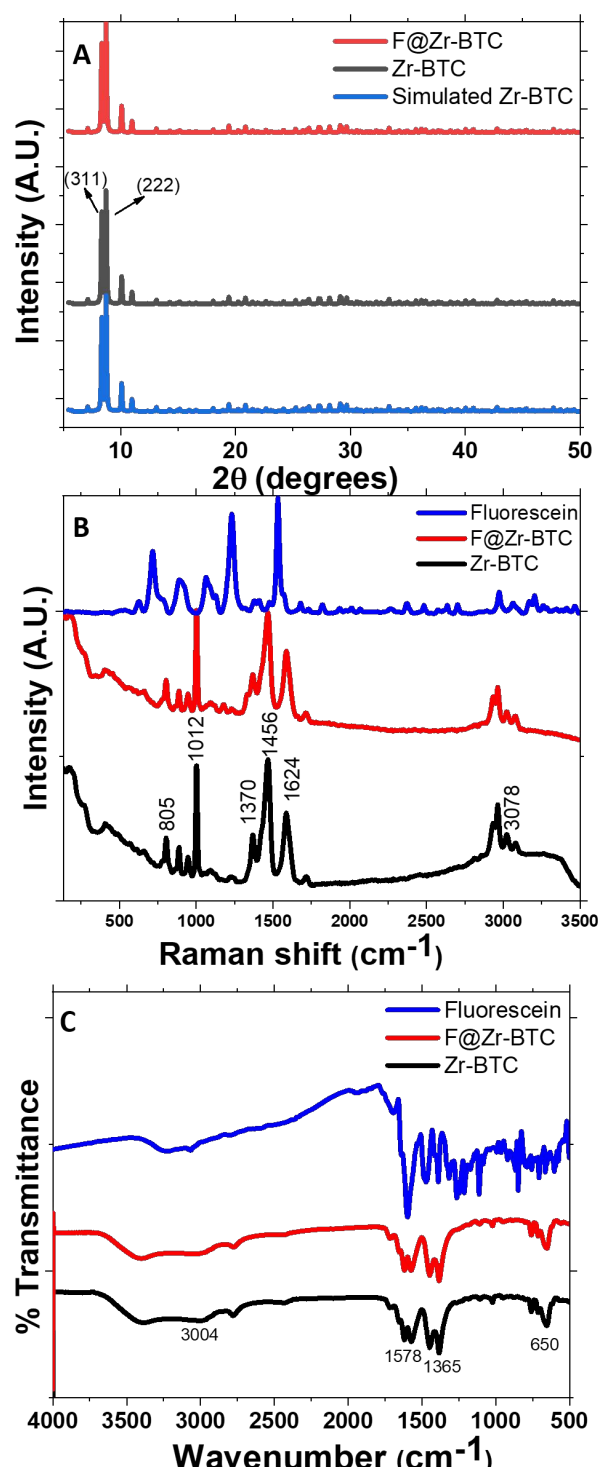


Figure 3. Structural characterization of Fluorescein (blue), Zr-BTC (black) and F@Zr-BTC (red): (a) Powder X-ray diffraction patterns with comparison to that of simulated Zr-BTC (sky blue), (b) Raman vibrational spectra, and (c) FTIR spectra in transmission mode.

The BET measurements show a loss in the surface area of the pristine Zr-BTC upon the Fluorescein encapsulation process. The pristine Zr-BTC has a surface area of $987 \text{ m}^2/\text{g}$. After encapsulating Fluorescein into Zr-BTC voids, the surface area is

reduced to $815 \text{ m}^2/\text{g}$ which is 17.5 % reduction in surface area which may confirm the encapsulation of Fluorescein. The adsorption-desorption isotherms of N_2 on Zr-BTC (black) and F@Zr-BTC (red) at 77 K are shown in Figure 4(a). The N_2 isotherm of F@Zr-BTC is lower than that of the original Zr-BTC, indicating that the surface area of F@Zr-BTC is smaller than that of original Zr-BTC, and becomes gradually small with Fluorescein loading. Fluorescence emission spectra in Figure 4(b) provide evidence of host-guest intermolecular interactions responsible for the red-shifted emission spectrum of F@Zr-BTC. The maximum emission peak of Zr-BTC at $\sim 500 \text{ nm}$ has been redshifted by $\sim 34 \text{ nm}$ to a longer wavelength of $\sim 534 \text{ nm}$ with higher intensity, which occurs upon encapsulation of Fluorescein guests inside Zr-BTC void. Moreover, the observed intensity enhancement and redshifted emission may attribute to the complexing between Zr and incorporated Fluorescein within F@Zr-BTC structure.⁵²⁻⁵⁴ This phenomenon may lead to tuning quenching selectivity of Fluorescein.

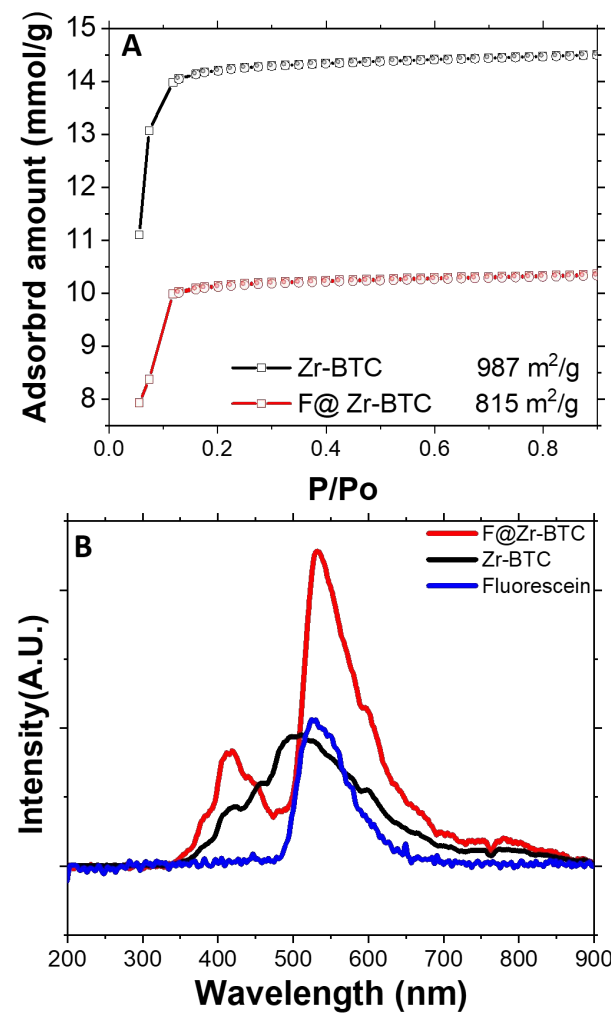


Figure 4. (a) N_2 adsorption (line)-desorption (open symbols) isotherms for Zr-BTC (black) and F@Zr-BTC (red) at 77 K (b) Fluorescence emission spectra of F@Zr-BTC (red), Zr-BTC (black) and, Fluorescein (blue) excited at $\lambda_{\text{ex}} = 470 \text{ nm}$.

3.2 CEES detections

Upon excitation at 470 nm, the F@Zr-BTC emits the strong yellowish green that can be quenched dramatically after the addition of CEES. F@Zr-BTC is expected to enable the selective and sensitive fluorescence detection of electron-rich CEES compound. All fluorescence-sensing measurements are performed by the dispersion of F@Zr-BTC nanocrystals in an ethanolic media because it is an environmentally friendly solvent. Fluorescein encapsulation greatly enhances the fluorescence spectrum of F@Zr-BTC as shown in Figure 4(b). Moreover, the electron deficient properties of Fluorescein have an effect on the electronic interaction between the analyte (CEES) and the sensing material (F@Zr-BTC). Upon addition of CEES compounds to solutions of F@Zr-BTC, fluorescence is quenched. As shown in Figure 5(a), the fluorescence emission spectra of ethanolic solutions containing 1 mg/mL of F@Zr-BTC are measured as a function of CEES concentrations ranging from 50 ppb to 4 ppm. The fluorescence quenching increases with increasing the CEES concentrations. The fluorescence quenching is defined as in the equation (1) where I is the maximum fluorescence intensity after exposure to CEES and I_0 is the maximum fluorescence intensity of the F@Zr-BTC before exposure. Alternatively, the fluorescence quenching response also follows the Stern-Volmer equation shown in equation (2) where K_{sv} is the Stern-Volmer coefficient and $[Q]$ is the molar concentration of the analyte. A K_{sv} value of 15945 M^{-1} is obtained. The limit of detection (LOD) can then be calculated with equation (3) where σ is the standard deviation of 4 sensors. The LOD for CEES is determined to be 0.212 nM.

$$\text{Fluorescence Quenching} = 1 - \frac{I}{I_0} \quad (1)$$

$$\frac{I_0}{I} = 1 + K_{sv}[Q] \quad (2)$$

$$LOD = 3 \frac{\sigma}{K_{sv}} \quad (3)$$

Figure 5(b) inset shows the linearity range, from 50 to 1000 ppb of this sensing material. After curve fitting, the best linear fitting corresponds to an R^2 of 0.968 at lower CEES concentrations that is attributed to either static or dynamic quenching. A nonlinear behavior is noticed at higher concentrations of CEES (Figure 5(b)), which may be attributed to a self-absorption or an occurrence of an energy transfer process between CEES and F@Zr-BTC. This sensing material also shows good selectivity to CEES as shown in Figure 5(c) and (d) compared to other analytes like 2-mercapto ethanol and H₂S which are containing sulfur and DMMP which is another CWA simulant.

The operating temperature and LOD comparisons with other sensing materials are shown in Table 1. The advantages of this work include the rapid and facile synthesis of sensing materials, room temperature operation, and higher sensitivity and selectivity. We demonstrated the selectivity of our sensing material (F@Zr-BTC) with sulfur containing chemicals and another CWA simulant dissolved in ethanolic solution. By comparison, other works demonstrated the selectivity of their nanomaterials with NO₂, NO, CO^{1,15} or NH₃, DMMP, H₂S⁵⁵ or various vapors such as methane acid, acetone, dichloroethane, dioxane, methanol etc⁵⁶.

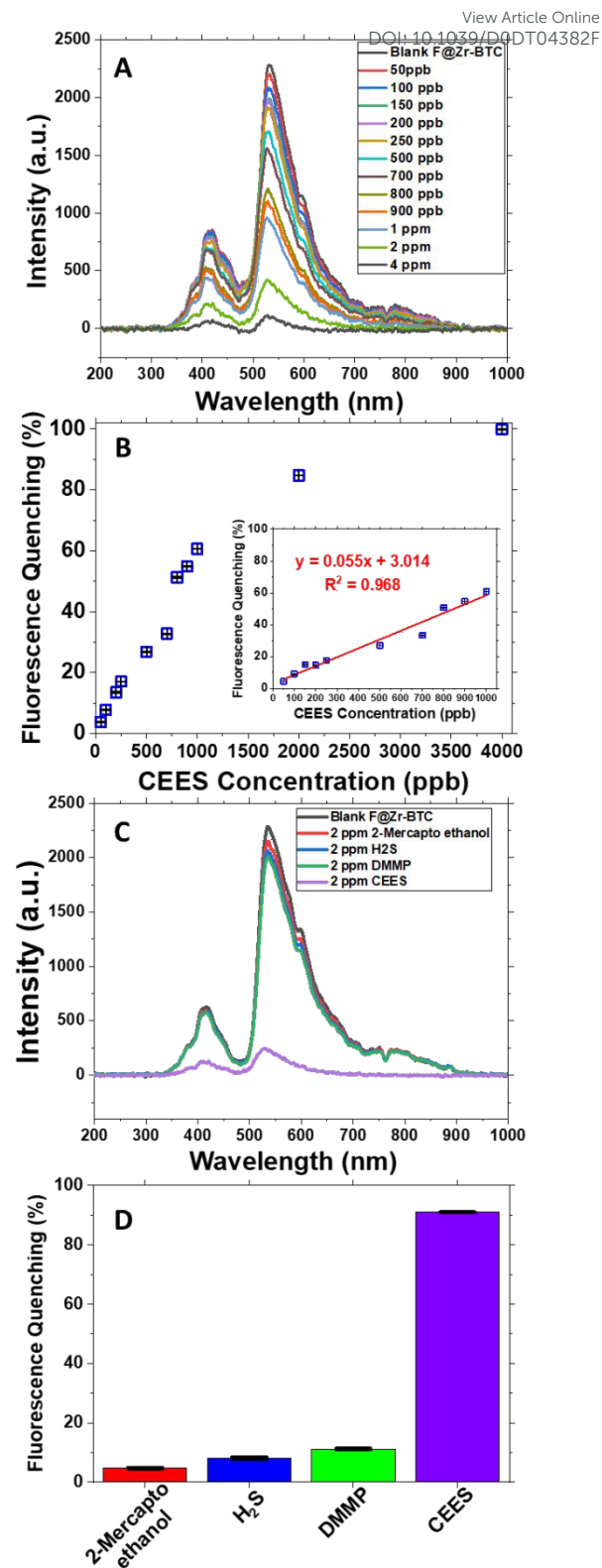


Figure 5. (a) Fluorescence emission spectra upon incremental addition of CEES ($\lambda_{\text{ex}} = 470\text{ nm}$). (b) Fluorescence quenching with ethanolic solution of F@Zr-BTC at different CEES concentrations from 50 ppb to 4 ppm. The inset shows a linear fitting curve (red) at lower concentration range. Error bars are calculated from the standard deviation of 4 sensors. (c) Fluorescence emission spectra upon addition of various

ARTICLE

Journal Name

analytes at 2 ppm concentration. (d) Fluorescence quenching comparison graph showing the chemical selectivity of F@Zr-BTC to CEES. Error bars are calculated from the standard deviation of 4 sensors.

Table 1. Comparison table of CEES sensors.

Sensing Material	Operating Temperature (°C)	Limit of Detection (ppm)	Ref
Polyepichlorohydrin	19	0.59	[55]
(4,7-bis(4-aminophenyl)-1H-benzimidazole-2-yl)ethan-1-ol with 1,3,6,8-tetrakis(4-formylphenyl)pyrene covalent organic framework	40	0.96	[56]
Al-doped and undoped ZnO quantum dots	450	20	[1]
Al-doped and undoped ZnO nanoparticles	500	20	[15]
F@Zr-BTC	20	0.048	This work

3.3 Sensing Mechanism

It has been reported that a single CEES molecule diameter is approximately 6.98 Å⁵⁷ which is smaller than the pore size of Zr-BTC. Therefore, adsorption is a likely mechanism. In addition, the CEES sensing mechanism has been commonly reported as a donor-acceptor electron transfer.⁷ The electron-rich CEES donates electrons to the electron deficient F@Zr-BTC as illustrated in Figure 6. The presence of Fluorescein inside Zr-BTC voids accepts the electrons from CEES molecule. Here it may be suggested that Zr-BTC acts as a surface adsorbent for CEES⁵⁸ which enables the electron transfer from CEES molecule (electron rich) to Fluorescein guest (electron deficient) which cause a dramatic quenching effect. It is worth mentioning that the no complex formation occurs during this process, the quenching typically occurs during the diffusion of CEES molecules towards the F@Zr-BTC surface which enables charge transfer and consequently lower the fluorescence intensity. Optical detection methods for CEES are not common due to low electrophilicity and lack of traditional molecular recognition sites such as hydrogen-bond acceptor or donor groups.⁵⁹ Dithiol, acting as an open chain receptor, has previously been used to overcome these problems.⁵⁹ However, thiols can also have harmful health effects which leads to the need for alternative methods.⁶⁰ CEES often decomposes into ClCH₂CH₂⁻ and ·SCH₂CH₃ which have Lewis base characteristics due to the end chlorine and sulfur groups.¹ This results in a high affinity for Lewis acidic sites such as the open metal ion sites on F@Zr-BTC.

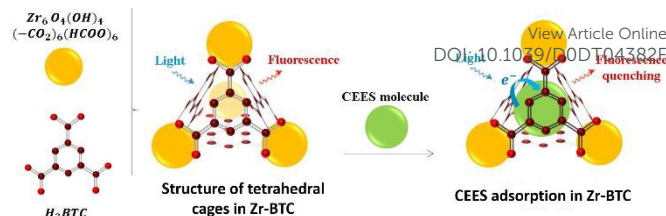


Figure 6. Schematic illustration of charge transfer complex interactions between F@Zr-BTC and CEES molecule.

4. Conclusions

In conclusion, functionalized Zr-BTC (F@Zr-BTC) is successfully synthesized with rapid and facile encapsulation of Fluorescein into the voids of Zr-BTC. The facile, rapid, in-situ synthesis technique is demonstrated to form a highly fluorescent MOF under visible light irradiation. The F@Zr-BTC nanocrystal suspension is used as a fluorescent probe for trace amount of CEES detection. The sensing material's chemical selectivity to CEES is demonstrated over DMMP, H₂S and 2-mercapto ethanol. CEES concentrations ranging from 50 ppb to 4 ppm are tested and a strong linear relationship is noticed between 50 ppb and 1 ppm. The LOD of this sensing method is determined to be 48 ppb. Future work will be developing practical applications of this sensing material by incorporating the F@Zr-BTC into a paper for real-time CEES sensing in the field.

Conflicts of interest

There are no conflicts to declare.

Acknowledgements

The authors acknowledge the support of the Natural Sciences and Engineering Research Council of Canada (NSERC). S.H acknowledges Alberta Graduate Excellence Scholarship – International. D.W acknowledges Alberta Innovates Graduate Scholarship. O.A also acknowledges Egyptian Armed Force for the financial support.

References

- 1 J. H. Lee, H. Jung, R. Yoo, Y. Park, H. Lee, Y. S. Choe and W. Lee, Sensors Actuators B. Chem., 2019, **284**, 444–450.
- 2 T. Ghazanfari , S. K. Ardestani, M. Varmazyar, M. E. Doost, F. Heidari, Z. Kianmehr, R. Gharebaghi, R. Sedaghat, H. Ghasemi, M. M. Naghizadeh, M. Heshmati, M. R. Vaez-Mahdavi and S. Faghizadeh., Immunoregulation., 2018, **1**, 9-24.
- 3 B. Papirmeister, C.L. Gross, H. Meier, J.P. Petrali and J.B. Johnson, Fund Appl Toxicol., 1985, **5**, S134-S149.
- 4 V. Kumar and E. V. Anslyn, Chem. Sci., 2013, **4**, 4292-4297.
- 5 P. Asha, M. Sinha and S. Mandal, RSC Adv., 2017, **7**, 6691-6696.
- 6 Z.M. Hassan and M. Ebtekar, International Immunopharmacology., 2001, **1**, 605-610.

Journal Name

- 7 J. E. Mondloch, M. J. Katz, W. C. Isley, P. Ghosh, P. Liao, et al., *Nat Mater.*, 2015, **14**, 512-516.
- 8 R.S. Pilling, G. Bernhardt, C.S. Kim, J. Duncan, C.B. Crothers, et al., *Sens. Actuators B Chem.*, 2003, **96**, 200–214.
- 9 M.A. Makinen, O.A. Anttalainen, M.E.T. Sillanpaa, *Anal. Chem.*, 2010, **82**, 9594–9600.
- 10 N. Taranenko, J. Pierre, D. Stokes, T. V. Dinh, J. Raman Spectrosc., 1996, **27**, 379–384.
- 11 D. Lee, S. Kim, I. Chae, S. Jeon, T. Thundat, *Appl. Phys. Lett.*, 2014, **104**, 141903.
- 12 F. Petersson, P. Sulzer, C.A. Mayhew, P. Watts, A. Jordan, L. Mark, T.D. Mark, *Rapid Commun. Mass Spectrom.*, 2009, **23**, 3875–3880.
- 13 Y. Sun, K. Y. Ong, *Detection technologies for Chemical Warfare Agents and Toxic Vapors*, CRC Press, Boca Raton, Florida, 1st edn, 2005, p. 272.
- 14 N.R. Brletich, M.J. Waters, G.W. Bowen and M.F. Tracy, *Worldwide Chemical Detection Equipment Handbook*, Chemical and Biological Defense Information Analysis Center, Maryland, 1995.
- 15 R. Yoo, D. Lee, S. Cho, and W. Lee, *Sensors Actuators B Chem.*, 2018, **254**, 1242-1248.
- 16 B. Singh, T.H. Mahato, A.K. Srivastava, G.K. Prasad , K. Ganeshan , et al., *J Hazard Mater.*, 2011, **190**, 1053-1057.
- 17 T.J. Bandosz, M. Laskoski, J. Mahle, G. Mogilevsky, G.W. Peterson, et al., *J Phys Chem C.*, 2012, **116**, 11606-11614.
- 18 R. S. Vemuri, P. D. Armatis , J. R. Bontha, B. P. McGrail, R. K. Motkuri, *J Bioterror Biodef*, 2015, **6**, 137.
- 19 J. A. Greathouse, N. W. Ockwig, L. J. Criscenti, T. R. Guilinger, P. Pohl, et al., *Phys Chem Chem Phys.*, 2012, **12**, 12621-12629.
- 20 Y. Liu, A. J. Howarth, J. T. Hupp and O. K. Farha, *Angew. Chem. Int. Ed.*, 2015, **54**, 9001-9005.
- 21 E. M. Dias, C. Petit, *J. Mater. Chem. A*, 2015, **3**, 22484-22506.
- 22 B. Liu, K. Vikrant, K-H Kim, V. Kumar and S. K. Kailasa, *Environ. Sci.: Nano*, 2020, **7**, 1319-1347.
- 23 Y. Liu, A. J. Howarth, N. A. Vermeulen, S.-Y. Moon, J. T. Hupp and O. K. Farha, *Coord. Chem. Rev.*, 2017, **346**, 101-111.
- 24 S. Wang, L. Bromberg, H. Schreuder-Gibson and T. A. Hatton, *ACS Appl. Mater. Interfaces*, 2013, **5**, 1269–1278.
- 25 P. Li, R. C. Klet, S. Y. Moon, T. C. Wang, P. Deria, A. W. Peters, B. M. Klahr, H. J. Park, S. S. Al-Juaid, J. T. Hupp and O. K. Farha, *Chem. Commun.*, 2015, **51**, 10925–10928.
- 26 C. F. Pereira, Y. Liu, A. J. Howarth, F. Figueira, J. Rocha, J. T. Hupp, O. K. Farha, J. P. C. Tome, F. A. A. Paz, *ACS Appl. Nano Mater.*, 2019, **2**, 465–469.
- 27 I. Stassen, B. Bueken, H. Reinsch, J.F.M. Oudenhoven, D. Wouters, J. Hajek, V. V. Speybroeck, N. Stock, P.M. Vereecken, R. V. Schaijk, D. D. Vosa, R. Ameloot, *Chem. Sci.*, 2016, **7**, 5827-5832.
- 28 G.Y Wang, C. Song, D. M Kong, W. J. Ruan, Z. Chang, Y. Li, J. Mater. Chem. A, 2014, **2**, 2213–2220.
- 29 A. Lan, K. Li, H. Wu, D. H. Olson, T. J. Emge, W. Ki, M. Hong, J. Li, *Angew. Chem. Int. Ed.*, 2009, **48**, 2334 –2338.
- 30 W. Xie, S. R. Zhang, D. Y. Du, J. S. Qin, S. J. Bao, J. Li, Z. M Su, W. W He, Q. Fu, Y. Q. Lan, *Inorg. Chem.*, 2015, **54**, New Article Online 3290–3296. DOI: 10.1039/DODT04382F
- 31 J. Dong, D. Zhao, Y. Lu, W-Y. Sun, *J. Mater. Chem. A*, 2019, **7**, 22744.
- 32 Y. Bai, Y. Dou, L. H. Xie, W. Rutledge, J. R. Li, H.C. Zhoub, *Chem.Soc.Rev.*, 2016, **45**, 2327-2367.
- 33 J. Jiang, et al., *J. Am. Chem. Soc.*, 2014, **136**, 12844-12847.
- 34 Y. Pu, et al., *Picosecond polarization spectroscopy of fluorescein attached to different molecular volume polymer influenced by rotational motion*. SPIE OPTO, 8258 (2012) SPIE.
- 35 R. Sjöback, J. Nygren, and M. Kubista , *Spectrochimica Acta Part A: Molecular and Biomolecular Spectroscopy.*, 1995, **51**, L7-L21.
- 36 L. Ullah, et al., *Science China Chemistry.*, 2018, **61**, 402-411.
- 37 B. Seoane, S. Castellanos, A. Dikhtarenko, F. Kapteijn, J. Gascon, *Coordination Chemistry Reviews*, 2016, **307**, 147-187.
- 38 R.S. Forgan, *Chem. Sci.*, 2020, **11**, 4546-4562
- 39 C.V. McGuire, R.S. Forgan, *Chem. Comm.*, 2015, **51**, 5199-5217.
- 40 Y. Peng, et al., *Nature Communications.*, 2018, **9**, 187-196.
- 41 H.-H. Mautschke, et al., *Catalysis Science & Technology.*, 2018, **8**, 3610-3616.
- 42 C. Ardila-Suárez, et al., *CrystEngComm.*, 2019, **21**, 1407-1415.
- 43 D.B. Dwyer, et al., *ACS Appl. Mater. Interfaces*, 2018, **10**, 25794-25803.
- 44 W. Liang, et al., *CrystEngComm.*, 2014, **16**, 6530-6533.
- 45 J. Xu, et al., *New Journal of Chemistry.*, 2019, **43**, 4092-4099.
- 46 Abuzalat, O., et al., *Nanoscale*, 2020, **12**, 13523-13530.
- 47 X. Fu, *J. Solid State Chem.*, 2018, **26**, 35-41.
- 48 A.K. Chaudhari, M.R. Ryder, and J.-C. Tan, *Nanoscale.*, 2016, **8**, 6851-6859.
- 49 H. Kaur, et al., *Journal of Drug Delivery Science and Technology.*, 2017, **41**, 106-112.
- 50 D. Yan, et al., *ChemPlusChem*, 2012, **77**, 1112-1118.
- 51 B. Rungtaweevoranit, et al., *Nano letters.*, 2016, **12**, 7645-7649.
- 52 W.-J. Wang, L. Hao, C.-Y. Chen, Q.-M. Qiu, K. Wang, J.-B. Song, H.J.R.a. Li, *RSC Adv.*, 2017, **7**, 20488-20493.
- 53 S. Goswami, D. Sen, N.K.J.O.L. Das, *Organic Letters*. 2010, **12**, 856-859.
- 54 K. Shimamoto, K.J.N.o. Hanaoka, *Nitric Oxide*, 2015, **30**, 72-9.
- 55 Y. Pan, N. Mu, B. Liu, B. Cao, W. Wang and L. Yang, *Sensors*, 2018, **18**, 2977.
- 56 Z. H. He, S. D. Gong, S. L. Cai, Y.L. Yan, G. Chen, X.L. Li, S. R. Zheng, J. Fan, and W. G. Zhang, *Cryst. Growth Des.*, 2019, **19**, 3543-3550.
- 57 A. Roy, A. K. Srivastava, B. Singh, D. Shah, T. H. Mahatoa, and A. Srivastava, *Dalton Trans.*, 2012, **41**, 12346-12348.
- 58 Ploskonka, A.M. and J.B. DeCoste, *ACS Appl. Mater. Interfaces*, 2017, **9**, 21579-21585.
- 59 V. Kumar, E. V. Anslyn, *J. Am. Chem. Soc.*, 2013, **135**, 6338-

ARTICLE

Journal Name

6344.
60 L. Włodek, *Pol. J. Pharmacol.*, 2002, **54**, 215–223.

[View Article Online](#)
DOI: 10.1039/D0DT04382F